SIMULTANEOUS BAYESIAN COMPRESSIVE SENSING AND BLIND DECONVOLUTION

Leonidas Spinoulas^a, Bruno Amizic^a, Miguel Vega^b, Rafael Molina^{c*}, and Aggelos K. Katsaggelos^{a†}

^{a} Dept. of Electrical Engineering and Comp. Sc., Northwestern University, Evanston, IL 60208, USA
^{b} Dept. Lenguajes y Sistemas Informáticos, Univ. de Granada, 18701 Granada, Spain
^{c} Dept. Ciencias de la Computación e I. A., Univ. de Granada, 18071 Granada, Spain
leonisp@u.northwestern.edu, amizic@northwestern.edu, mvega@ugr.es, rms@dcsai.ugr.es, aggk@eecs.northwestern.edu

ABSTRACT

The idea of compressive sensing in imaging refers to the reconstruction of an unknown image through a small number of incoherent measurements. Blind deconvolution is the recovery of a sharp version of a blurred image when the blur kernel is unknown. In this paper, we combine these two problems trying to estimate the unknown sharp image and blur kernel solely through the compressive sensing measurements of a blurred image. We present a novel algorithm for simultaneous image reconstruction, restoration and parameter estimation. Using a hierarchical Bayesian modeling followed by an Expectation-Minimization approach we estimate the unknown image, blur and hyperparameters of the global distribution. Experimental results on simulated blurred images support the effectiveness of our method. Moreover, real passive millimeter-wave images are used for evaluating the proposed method as well as strengthening its practical aspects.

Index Terms— Compressive sensing, blind deconvolution, bayesian method, blur kernel, passive millimeter wave images.

1. INTRODUCTION

Compressive sensing (CS) has become a fast growing field in recent years due to its interesting theoretical nature and its potential aid in numerous practical applications [1, 2]. CS uses a small number of random incoherent linear projections of a signal (e.g., an image) and tries to reconstruct the original signal through a reconstruction algorithm. It is basically an efficient sampling scheme which avoids collecting redundant information exploiting the sparsity inherent in many signals (e.g., natural images, passive millimeter-wave images).

Numerous methods have been proposed for the effective solution of the CS problem. Some of them are based on energy minimization, while others, like the one presented here, follow a Bayesian framework [3, 4, 5, 6].

CS has proven to be useful in capturing images of low-energy radiation such as passive millimeter-waves (PMMW), [3, 7]. The millimeter-wave (MMW) regime lies in the microwave spectrum in the frequency band between 30 and 300 GHz and has various advantages over conventional (e.g., visible light or infrared) imaging under adverse conditions. In environments dominated by clouds, fog, smoke, rain, snow or dust-storms, PMMW radiation is attenuated multiple orders of magnitude less than visual or infrared radiation [8]. The ability to capture radiation in low-visibility conditions has led to numerous applications of MMW technology over the course of years [8]. Furthermore, advances in millimeter-wave radiometry and integrated circuit design [9] extended their use while technological breakthroughs led to the development of passive-millimeter wave video devices [10]. More recently, active and passive millimeter-wave scanners have been successfully used in airports to detect a broad range of concealed threats [11].

The main reason for exploiting CS techniques in MMW applications is the high cost of radiometers [12], collecting the incoming radiation of a scene. In a non-CS setup, one radiometer is required for the formation of a pixel in the acquired image, leading to expensive devices even for low resolution imaging. Therefore, one would wish to minimize the required number of radiometers while still obtaining comparable imaging quality. On the other hand, such reduction leads to increased acquisition time since the available radiometers are now responsible for multiple sequential collective CS measurements which require long integration intervals for acceptable signal-to-noise ratio (SNR). Recently, CS PMMW imaging systems have been proposed to overcome this problem by reducing the amount of required measurements utilizing efficient CS matrices (masks) and effective reconstruction algorithms ([3, 7]).

As in most imaging systems, CS PMMW imagers utilize lenses to focus the low-energy radiation of the scene. The point spread function (PSF) of these lenses usually introduces blur in the acquired measurements or equivalently the reconstructed image. Examples of PMMW images captured through our proposed CS imager were presented in [3], and more can be found in section 4. It is apparent that all images

---

have been degraded not only with noise but also with a considerable amount of blur. Moreover, most MMW systems have narrow depth-of-field [13], the distance over which an object is considered in focus. Therefore, if the imager is not in the appropriate distance or if non-stationary targets are observed, blurring effects also dominate the scene (example images can be found in [13, 14]). Hence, for improved quality PMMW imaging, it is essential to compensate for the blur introduced by CS PMMW systems either by including a known blur in the reconstruction algorithm or by estimating it during the reconstruction process forming a simultaneous reconstruction and restoration problem.

The image restoration problem has been studied exhaustively in the literature where various methods for blind deconvolution (BD) or deblurring have been presented. Recent algorithms have afforded dramatic progress, yet many aspects of the problem remain challenging and hard to understand [15, 16, 17, 18]. A standard formulation of the image degradation model is given in matrix-vector form by:

$$\mathbf{g} = \mathbf{H}\mathbf{x} + \mathbf{n}, \tag{1}$$

where $\mathbf{g}$ is the $N \times 1$ observation vector, vector $\mathbf{x}$ ($N \times 1$) represents the lexicographically ordered unknown image, $\mathbf{n}$ is an $N \times 1$ acquisition noise vector and $\mathbf{H}$ corresponds to the $N \times N$ blurring matrix constructed by the blurring PSF (denoted by $\mathbf{h}$ in vector form). The degradation represented by the blurring matrix $\mathbf{H}$ is generally nonlinear (due to saturation, quantization, etc.) and spatially varying (lens imperfections, nonuniform motion, etc.) [15]. However, most of the relevant work approximates the degradation process by a linear spatially invariant (LSI) system, where the original image is convolved by the blurring kernel (PSF). In this case the matrix $\mathbf{H}$ can be easily constructed as a block circulant matrix with circulant blocks. When $\mathbf{H}$ is known we refer to a non-blind deblurring problem, otherwise the deblurring is called blind.

The goal of this paper is to perform CS measurements of an unknown blurred image and try to reconstruct it as well as restore the unknown blurring kernel. The rest of this paper is organized as follows. In section 2 the Bayesian modeling of the problem is introduced. Inference is presented in section 3 and experiments on both synthetic and real PMMW images are conducted in section 4. Finally, conclusions are drawn in section 5.

2. BAYESIAN MODELING

2.1. Observation Model

Assuming that the image is degraded by a blurring matrix $\mathbf{H}$ we perform $M \ll N$ measurements using a CS matrix $\mathbf{\Phi}$ of size $M \times N$. Therefore, the full observation model results in:

$$\mathbf{y} = \mathbf{\Phi}\mathbf{H}\mathbf{x} + \mathbf{n}, \tag{2}$$

where $\mathbf{y}$ is the $M \times 1$ CS measurement vector and $\mathbf{n}$ is an $M \times 1$ acquisition noise vector.

The noise component $\mathbf{n}$ is modeled, using the Gaussian noise assumption, by the conditional distribution:

$$p(\mathbf{y}|\mathbf{x}, \mathbf{h}, \beta) \propto \beta^{M/2} \exp\left[-\frac{\beta}{2}\|\mathbf{y} - \mathbf{\Phi}\mathbf{H}\mathbf{x}\|^2\right] \tag{3}$$

where β is the inverse noise variance (precision).

2.2. Prior Modeling

The prior used for the image has been previously presented in [3, 19] and in an earlier form in [20]. The prior assumes that high-pass filtering of the image $\mathbf{x}$ produces an image with most pixels zero or negligibly small. It basically captures the sparse edges of an image using various directional derivative filters and is, in effect, similar to a Total-Variation (TV) prior with additional degrees of freedom. This behavior is modeled using a sparsity inducing zero-mean multivariate Gaussian distribution that combines the constraints given by a set of L high-pass filters $\mathbf{D}_k$ as follows:

$$p(\mathbf{x}|\{\mathbf{A}_k\}) \propto |\mathbf{\Sigma}_F|^{-1/2} \exp\left[-\frac{1}{2}\mathbf{x}^T \left(\mathbf{\Sigma}_F^{-1}\right) \mathbf{x}\right]$$

$$\mathbf{\Sigma}_F^{-1} = \sum_{k=1}^{L} \mathbf{D}_k^T \mathbf{A}_k \mathbf{D}_k, \tag{4}$$

where $\mathbf{D}_k$, $k = 1, 2, ..., L$ are $N \times N$ high-pass filters, and $\mathbf{A_k}$'s are $N \times N$ diagonal matrices containing the hyperparameters α_{ki} associated with the inverse variance (precision) of the response of each corresponding filter operator $\mathbf{D}_k$ for any given pixel i. Therefore, $\mathbf{A}_k = diag(\alpha_{ki})$, $i = 1, 2, ..., N$.

As presented in [19], the advantage of this image prior is twofold. First, it avoids the selection of any specific sparsity promoting shape for the prior distribution, since such information is inherited in the precision hyperparameters. Second, by choosing a Gaussian distribution we are able to seek a tractable inference mechanism.

For the blur prior we use the well-known simultaneous autoregressive (SAR) model which has been used extensively in the literature:

$$p(\mathbf{h}|\gamma) \propto \gamma^{N_b/2} \exp\left[-\frac{\gamma}{2}\|\mathbf{C}\mathbf{h}\|^2\right], \tag{5}$$

where $\mathbf{C}$ denotes the discrete laplacian operator, γ is the precision of the Gaussian distribution and N_b is the support of the blur. The SAR model is very efficient in estimating smooth PSFs. Experimental results, [21], have shown that PMMW systems have smoothly varying PSFs, hence supporting our choice of prior.

Finally, the hyperparameters are assigned uniform distributions such that:

$$p(\beta) \propto const, \; p(\gamma) \propto const, \; p(\alpha_{ki}) \propto const, \tag{6}$$

for $k = 1, \ldots, L, i = 1, \ldots, N$.

3. BAYESIAN INFERENCE

Using equations (3), (4), (5) and (6), the joint distribution $p(\mathbf{y}, \mathbf{h}, \mathbf{x}, \{\mathbf{A}_k\}, \beta, \gamma)$ is defined as:

$$p(\mathbf{y}, \mathbf{h}, \mathbf{x}, \{\mathbf{A}_k\}, \beta, \gamma) =$$
$$p(\mathbf{y}|\mathbf{h}, \mathbf{x}, \beta)p(\mathbf{x}|\{\mathbf{A}_k\})p(\mathbf{h}|\gamma)p(\beta)p(\gamma)\prod_{k=1}^{L}\prod_{i=1}^{N}p(\alpha_{ki}) \quad (7)$$

We utilize the Expectation-Maximization (EM) framework to solve for the best image and blur following a similar approach to [17]. This algorithm alternates between two separate steps. In the *E-step* one solves a non-blind deconvolution problem estimating the mean image and its covariance given the current blur kernel. In the *M-step* one solves for the optimal blur kernel given the image and its covariance around it.

In the *E-step* the image is estimated as a multivariate Gaussian distribution $q(x) = \mathcal{N}(\mathbf{x}|\mu_{\mathbf{x}}, \Sigma_{\mathbf{x}})$ with parameters:

$$\mu_{\mathbf{x}} = \Sigma_{\mathbf{x}}\beta\mathbf{H}^T\mathbf{\Phi}^T\mathbf{y} \quad (8)$$

$$\Sigma_{\mathbf{x}}^{-1} = \beta\mathbf{H}^T\mathbf{\Phi}^T\mathbf{\Phi}\mathbf{H} + \sum_{k=1}^{L}\mathbf{D}_k^T\mathbf{A}_k\mathbf{D}_k \quad (9)$$

In the *M-step*, we estimate $\mathbf{h}$ minimizing:

$$E_{q(\mathbf{x})}\left[\frac{\beta}{2}\|\mathbf{y} - \mathbf{\Phi}\mathbf{H}\mathbf{x}\|^2\right] + \frac{\gamma}{2}\|\mathbf{C}\mathbf{h}\|^2 \quad (10)$$

Equation (10) is quadratic on the unknown $\mathbf{h}$ and its solution is:

$$\hat{\mathbf{h}} = \arg\min_{\mathbf{h}}\frac{1}{2}\mathbf{h}^T A_{\mathbf{h}}\mathbf{h} - b_{\mathbf{h}}^T\mathbf{h}, \quad s.t. \ \mathbf{h} \geq 0 \quad (11)$$

with:

$$A_{\mathbf{h}}(i_1, i_2) = \beta\sum_{k=1}^{N}\sum_{l=1}^{N}\phi_k^T\phi_l z(k - i_1, l - i_2) + \gamma\tilde{C}(i_1, i_2) \quad (12)$$

$$z(k-i_1, l-i_2) = E_{q(\mathbf{x})}\left[x(k - i_1)x(l - i_2)\right] = $$
$$= \mu_{\mathbf{x}}(k - i_1)\mu_{\mathbf{x}}(l - i_2) + \Sigma_{\mathbf{x}}(k - i_1, l - i_2) \quad (13)$$

$$b_{\mathbf{h}}(i_1) = \beta\sum_{k=1}^{N}\mu_{\mathbf{x}}(k - i_1)\mathbf{y}^T\phi_k$$
$$= \beta\sum_{k=1}^{N}\mu_{\mathbf{x}}(k - i_1)\sum_{i=1}^{M}y(i)\phi_k(i), \quad (14)$$

where i_1, i_2 denote lexicographically ordered blur kernel indices, $\phi_k(i)$ denotes the i-th component of the k-th column of $\mathbf{\Phi} = [\phi_1, \ldots, \phi_N]$ and $\tilde{C} = \mathbf{C}^T\mathbf{C}$.

The update for the parameters α_{ki} is given (see [19]) by:

$$\alpha_{ki}^{(l+1)} = \alpha_{ki}^{(l)}\frac{\text{trace}\left[\Sigma_F\mathbf{D}_k^T\mathbf{J}^{ii}\mathbf{D}_k\right]}{\left(\mathbf{v}_{ki}^{(l)}\right)^2 + \text{trace}\left[\Sigma_{\mathbf{x}}\mathbf{D}_k^T\mathbf{J}^{ii}\mathbf{D}_k\right]}, \quad (15)$$

where $\mathbf{v}_k = \mathbf{D}_k\mu_{\mathbf{x}}$, $\mathbf{J}^{ii}$ is the single-entry matrix with only one at entry (i, i) and l denotes the iteration index. At the same time the precision parameters β and γ are estimated by:

$$\beta = M/\left(\|\mathbf{y} - \mathbf{\Phi}\mathbf{H}\mu_{\mathbf{x}}\|^2 + \text{trace}\left(\mathbf{H}^T\mathbf{\Phi}^T\mathbf{\Phi}\mathbf{H}\Sigma_{\mathbf{x}}\right)\right) \quad (16)$$

$$\gamma = N_b/\|\mathbf{C}\mathbf{h}\|^2 \quad (17)$$

The algorithm iterates between the unknown image estimation (8), the unknown blur estimation (11) and the estimation of the hyperparameters (15), (16) and (17) until a convergence criterion is met. Equations (13,15,16) require the explicit construction of the $N \times N$ covariance matrix $\Sigma_{\mathbf{x}}$ which is computationally demanding. Hence, as in [3, 19], we approximate it as a diagonal matrix whose elements are reciprocals of the diagonal elements of $\Sigma_{\mathbf{x}}^{-1}$.

4. EXPERIMENTAL RESULTS

In this section we present CS and BD on both synthetic and real PMMW images to demonstrate the performance of our algorithm. For the synthetic experiments we utilized the standard "Shepp-Logan" image which has similar appearance to common PMMW images. However, due to the computational complexity of the algorithm we use a smaller version of size 65×65 pixels. The image is blurred with a Gaussian-shaped function of variance 3.5 and white Gaussian noise is added to the CS measurements to obtain degraded observations with signal-to-noise ratio (SNR) 40dB.

For the real experiments we use PMMW images which constitute a practical reconstruction/restoration application for the proposed method. The real PMMW images were provided by the Argonne National Laboratory (ANL). The images have size 49×49 pixels.

For the synthetic experiments we employ six filters $\mathbf{D}_k$ (second order horizontal and vertical as well as first and second order diagonal) while for the real PMMW images only four first order (horizontal - vertical - diagonal) filters are utilized. The choice of filters was based on resulting image quality. The quantitative measure of performance for the synthetic experiments is the ISNR defined as $10\log_{10}(\|\mathbf{x} - \mathbf{x}_b\|^2/\|\mathbf{x} - \mu_{\mathbf{x}}\|^2)$ where $\mathbf{x}_b$ is the blurred image. The only qualitative measure utilized for the real experiments is visual inspection. For all experiments, the convergence criterion used for the termination of the algorithm is $\|\mathbf{x}^l - \mathbf{x}^{l-1}\|^2/\|\mathbf{x}^{l-1}\|^2 < 10^{-4}$ where l denotes the iteration number. Additionally, the support of the blur was set a priori to 17×17. All measurement vectors $\mathbf{y}$ are acquired through binary CS matrices to verify the applicability of the method in a real CS setup. The initial blur for all test cases is set to a Gaussian of variance 1 while the hyperparameters β and γ are given initial values 1 and 10^5, respectively. Finally, for all results reported here the covariance matrix, $\Sigma_{\mathbf{x}}$, was not utilized in the calculation of equation (13).
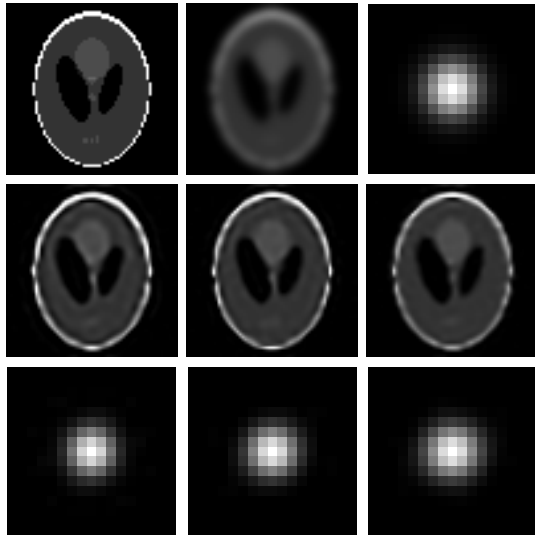
Fig. 1: Example restorations of the Shepp-Logan image. 1st row shows the original (left) and blurred (middle) images as well as the 17×17 original blur kernel; 2nd row shows the blind restoration results for 50%, 60% and 70% of CS measurements, respectively, from left to right; 3rd row shows the estimated blur kernels for each restoration, respectively. The corresponding ISNRs are reported in Table 1. Note that for illustration purposes (higher contrast) the intensity of the blur kernels has been normalized.

Table 1: ISNR values (in dB) for the blind and non-blind reconstruction of the Shepp-Logan image degraded by a Gaussian PSF of variance 3.5 at SNR = 40dB.

CS ratio	0.3	0.4	0.5	0.6	0.7	0.8
Blind	2.67*	2.98*	3.16	4.19	3.61	3.20
Non-Blind	3.73	3.94	3.88	4.39	4.23	4.30

The synthetic original, degraded and restored images, together with their corresponding blur kernels are presented in Fig. 1. Table 1 compares the resulting ISNR of the blind and non-blind reconstructions for various compressive ratios. The non-blind achievable ISNR is not necessarily improving while the percentage of measurements increases. This behavior can be explained due to the CS setting of the method, where performance depends on the particular selection of measurement matrices, which is random for each CS ratio. The blind case ISNR shows acceptable performance for CS ratios greater than 0.4 while exhibiting analogous fluctuations over increasing ratios. For lower percentages, the estimation of the blur may fail. However, empirical weighting of the hyperparameters β and γ has provided acceptable ISNRs as the ones reported in Table 1 with *. This leads us to the idea of using varying confidence weights to the hyperparameters based on the CS ratio, since, as the ratio reduces the problem becomes highly underdetermined. Further research is required and will be conducted towards this direction.

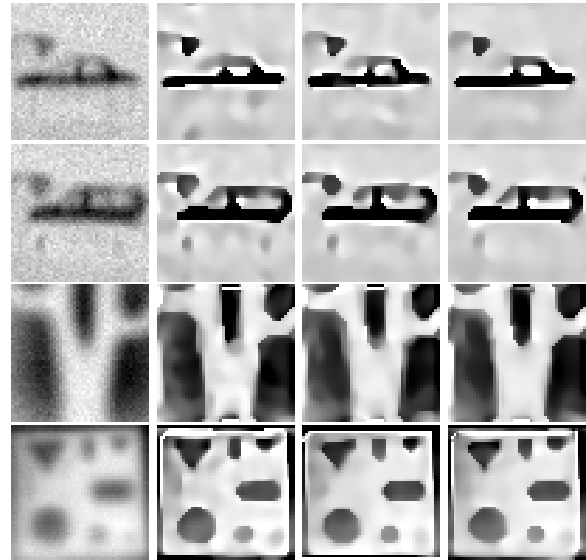The degraded and restored real PMMW images are pre-

Fig. 2: Example restorations of real PMMW images depicting cars, a pair of scissors and a metallic mask with hollow geometric shapes. 1st column represents the original uncompressed blurred observation; 2nd, 3rd, and 4th columns correspond to the resulting restoration for 40%, 60% and 80% of CS measurements, respectively.

sented in Fig. 2. Through our experiments we demonstrate that PMMW images are effectively enhanced, depicting the scene in higher detail. Moreover, the usage of first order filters results in piecewise-smooth images which effectively recover sharp edges (note the detection of the wheels of the second car or the circular geometric shape at the lower right corner of the metallic mask). Unfortunately, due to unavailability of equivalent simultaneous methods, no comparisons are reported. However, the CS reconstruction stage of the algorithm has been previously proven to provide superior performance compared to state-of-the-art TV-minimization schemes [3]. Hence, it is expected that a sequential reconstruction-deconvolution algorithm utilizing our proposed reconstruction step would provide improved restoration compared to other CS methods.

5. CONCLUSIONS

In this paper we proposed a novel algorithm for simultaneous compressive sensing reconstruction and blind deconvolution of images. The algorithm employs Bayesian modeling and the Expectation-Minimization approach to estimate an unknown sharp image and its blur kernel simultaneously. Simulations prove that solely compressive sensing measurements can potentially recover both the image and the degrading PSF. Furthermore, the method has practical applications in CS imaging setups such as for PMMW images whose restoration was presented here. The resulting images prove that modeling of the unknown blur kernel is desirable when restoring images obtained through a lens-based CS system.

6. REFERENCES

[1] Y. Tsaig and D.L. Donoho, "Compressed sensing," *IEEE Trans. Inform. Theory*, vol. 52, pp. 1289–1306, 2006.

[2] E.J. Candés, J. Romberg, and T. Tao, "Robust uncertainty principles: exact signal reconstruction from highly incomplete frequency information," *Information Theory, IEEE Transactions on*, vol. 52, no. 2, pp. 489 – 509, feb. 2006.

[3] S.D. Babacan, M. Luessi, L. Spinoulas, A.K. Katsaggelos, N. Gopalsami, T. Elmer, R. Ahern, S. Liao, and A. Raptis, "Compressive passive millimeter-wave imaging," in *Image Processing (ICIP), 2011 18th IEEE International Conference on*, sept. 2011, pp. 2705 –2708.

[4] S. Ji, Y. Xue, and L. Carin, "Bayesian compressive sensing," *Signal Processing, IEEE Transactions on*, vol. 56, no. 6, pp. 2346 –2356, june 2008.

[5] L. He and L. Carin, "Exploiting structure in wavelet-based bayesian compressive sensing," *Signal Processing, IEEE Transactions on*, vol. 57, no. 9, pp. 3488 – 3497, sept. 2009.

[6] M.W. Seeger and N. Hannes, "Compressed sensing and bayesian experimental design," in *Proceedings of the 25th international conference on Machine learning*, New York, NY, USA, 2008, ICML '08, pp. 912–919, ACM.

[7] N. Gopalsami, S. Liao, T. Elmer, A. Heifetz, and A. C. Raptis, "Compressive sampling in active and passive millimeter-wave imaging," in *Proc. 36th Int Infrared, Millimeter and Terahertz Waves (IRMMW-THz) Conf*, 2011, pp. 1–2.

[8] L. Yujiri, "Passive millimeter wave imaging," in *Proc. IEEE MTT-S Int. Microwave Symp. Digest*, 2006, pp. 98–101.

[9] H.P. Moyer, J.J. Lynch, J.N. Schulman, R.L. Bowen, J.H. Schaffner, A.K. Kurdoghlian, and T.Y. Hsu, "A low noise chipset for passive millimeter wave imaging," in *Proc. IEEE/MTT-S Int. Microwave Symp*, 2007, pp. 1363–1366.

[10] J.A. Lovberg, C. Martin, and V. Kolinko, "Video-rate passive millimeter-wave imaging using phased arrays," in *Proc. IEEE/MTT-S Int. Microwave Symp*, 2007, pp. 1689–1692.

[11] O. Martinez, L. Ferraz, X. Binefa, I. Gomez, and C. Dorronsoro, "Concealed object detection and segmentation over millimetric waves images," in *Proc. IEEE Computer Society Conf. Computer Vision and Pattern Recognition Workshops (CVPRW)*, 2010, pp. 31–37.

[12] N. Gopalsami, S. Bakhtiari, T. W. Elmer II, and A. C. Raptis, "Application of millimeter-wave radiometry for remote chemical detection," vol. 56, no. 3, pp. 700–709, 2008.

[13] J.N. Mait, D.A. Wikner, M.S. Mirotznik, J. van der Gracht, G.P. Behrmann, B.L. Good, and S.A. Mathews, "94-ghz imager with extended depth of field," *Antennas and Propagation, IEEE Transactions on*, vol. 57, no. 6, pp. 1713 –1719, june 2009.

[14] N.M. Joseph, D.A. Wikner, M.S. Mirotznik, and C. Fernandez-Cull, "New technologies to enable millimeter-wave imaging," in *Imaging Systems*. 2010, p. IMB4, Optical Society of America.

[15] S.D. Babacan, R. Molina, and A.K. Katsaggelos, "Variational bayesian blind deconvolution using a total variation prior," *Image Processing, IEEE Transactions on*, vol. 18, no. 1, pp. 12 –26, jan. 2009.

[16] A. Levin, Y. Weiss, F. Durand, and W.T. Freeman, "Understanding and evaluating blind deconvolution algorithms," in *Computer Vision and Pattern Recognition, 2009. CVPR 2009. IEEE Conference on*, june 2009, pp. 1964 –1971.

[17] A. Levin, Y. Weiss, F. Durand, and W.T. Freeman, "Efficient marginal likelihood optimization in blind deconvolution," in *Computer Vision and Pattern Recognition (CVPR), 2011 IEEE Conference on*, june 2011, pp. 2657 –2664.

[18] R. Fergus, B. Singh, A. Hertzmann, S.T. Roweis, and W.T. Freeman, "Removing camera shake from a single photograph," in *ACM SIGGRAPH 2006 Papers*, New York, NY, USA, 2006, SIGGRAPH '06, pp. 787–794, ACM.

[19] E. Vera, M. Vega, R. Molina, and A.K. Katsaggelos, "A novel iterative image restoration algorithm using nonstationary image priors," in *Image Processing (ICIP), 2011 18th IEEE International Conference on*, sept. 2011, pp. 3457 –3460.

[20] S.D. Babacan, R. Molina, and A.K. Katsaggelos, "Sparse bayesian image restoration," in *Image Processing (ICIP), 2010 17th IEEE International Conference on*, sept. 2010, pp. 3577 –3580.

[21] Y. Li, J.W. Archer, J. Tello, G. Rosolen, F. Ceccato, S.G. Hay, A. Hellicar, and Y.J. Guo, "Performance evaluation of a passive millimeter-wave imager," *Microwave Theory and Techniques, IEEE Transactions on*, vol. 57, no. 10, pp. 2391 –2405, oct. 2009.